Molecular Biology of the Cell
Vol. 10, 4327–4339, December 1999

Espin Contains an Additional Actin-binding Site in Its N Terminus and Is a Major Actin-bundling Protein of the Sertoli Cell–Spermatid Ectoplasmic Specialization Junctional Plaque

Bin Chen, Anli Li, Dennis Wang, Min Wang, Lili Zheng, and James R. Bartles*

Department of Cell and Molecular Biology, Northwestern University Medical School, Chicago, Illinois 60611

Submitted July 16, 1999; Accepted October 6, 1999
Monitoring Editor: Thomas D. Pollard

The espins are actin-binding and -bundling proteins localized to parallel actin bundles. The 837-amino-acid "espin" of Sertoli cell–spermatid junctions (ectoplasmic specializations) and the 253-amino-acid "small espin" of brush border microvilli are splice isoforms that share a C-terminal 116-amino-acid actin-bundling module but contain different N termini. To investigate the roles of espin and its extended N terminus, we examined the actin-binding and -bundling properties of espin constructs and the stoichiometry and developmental accumulation of espin within the ectoplasmic specialization. An espin construct bound to F-actin with an approximately threefold higher affinity (K_d = ~70 nM) than small espin and was ~2.5 times more efficient at forming bundles. The increased affinity appeared to be due to an additional actin-binding site in the N terminus of espin. This additional actin-binding site bound to F-actin with a K_d of ~1 μM, decorated actin stress fiber-like structures in transfected cells, and was mapped to a peptide between the two proline-rich peptides in the N terminus of espin. Espin was detected at ~4–5 × 10^6 copies per ectoplasmic specialization, or ~1 espin per 20 actin monomers and accumulated there coincident with the formation of parallel actin bundles during spermiogenesis. These results suggest that espin is a major actin-bundling protein of the Sertoli cell–spermatid ectoplasmic specialization.

INTRODUCTION

The espins constitute an emerging family of actin-binding and -bundling proteins (Bartles *et al.*, 1996, 1998). Outside of some relatively limited, yet nonetheless intriguing, sequence similarity to the forked proteins of *Drosophila* (Hoover *et al.*, 1993; Bartles *et al.*, 1996, 1998; Grieshaber and Petersen, 1999), the espins show no obvious resemblance to other actin-binding proteins. The founding member of the family, "espin," was identified as an 837-amino-acid protein localized to the parallel actin bundles in the submembranous plaque of the Sertoli cell ectoplasmic specialization (ES; espin = *e*ctoplasmic *sp*ecialization + -in) (Bartles *et al.*, 1996). (An unrelated protein with a very similar name, epsin, appeared in the literature beginning in 1998 [Chen *et al.*, 1998].)

* Corresponding author. E-mail address: j-bartles@nwu.edu
Abbreviations used: BHK, baby hamster kidney; ES, ectoplasmic specialization; GFP, green fluorescent protein; NTA, nitrilotriacetic acid.

A large body of evidence supports the hypothesis that the ES is an adhesive intercellular junction that anchors and positions the spermatid within the seminiferous epithelium throughout much of spermiogenesis (reviewed by Russell and Peterson, 1985; Vogl, 1989; Vogl *et al.*, 1991). Found at sites where the Sertoli cell plasma membrane makes close contact with the head of an elongating spermatid, the ES is characterized by a unique junctional plaque in which parallel actin bundles with hexagonally packed filaments are sandwiched between the Sertoli cell plasma membrane and an affiliated flattened cistern of endoplasmic reticulum (Figure 1; Russell and Peterson, 1985; Vogl, 1989; Vogl *et al.*, 1991). The parallel actin bundle layer of the ES junctional plaque is believed to act both as a scaffold that supports and stabilizes an adhesive domain within the overlying Sertoli cell plasma membrane and indirectly, via its connection to the cistern of endoplasmic reticulum, as a link to an underlying network of microtubles that may be responsible for changes in the depth of the ES–spermatid complex within the seminiferous epithelium (Russell and Peterson, 1985;

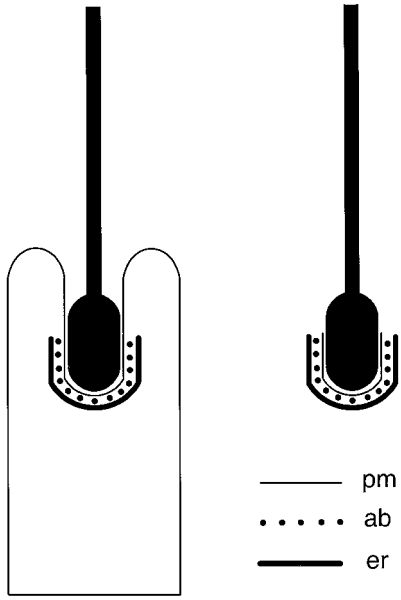

Figure 1. Simplified schematic diagram of an ES formed between a Sertoli cell and a late spermatid in section. pm, Sertoli cell plasma membrane; er, flattened cistern of endoplasmic reticulum; ab, actin bundles. Each dot represents a parallel actin bundle cut in cross section. (Left) In the seminiferous epithelium, the head of the spermatid is held within an invagination of the Sertoli cell, and the ES is found where the Sertoli cell plasma membrane makes close contact with acrosomal region of the spermatid head. (Right) After isolation by mechanical dissociation, the majority of late spermatids retain an ES, including junctional plaque, attached to their head.

Vogl, 1989, 1996; Vogl *et al*., 1991; Beach and Vogl, 1999). By analogy to the F-actin-rich plaques of other junctions, such as the focal adhesion (Schoenwaelder and Burridge, 1999) and the zonula adherens (Ben Ze'ev and Geiger, 1998), it is likely that the parallel actin bundle layer also serves as a repository for a specific complement of signaling and adapter proteins. Structures resembling ESs are also present within the junctional complex between neighboring Sertoli cells, where they may contribute to the integrity of the "blood–testis" barrier (Russell and Peterson, 1985; Vogl, 1989; Vogl *et al*., 1991).

In our initial characterization of espin, we determined that a maltose-binding protein fusion protein containing the C-terminal ~45% of espin bound to F-actin with high affinity in vitro (Bartles *et al*., 1996). When expressed ectopically in transiently transfected rodent fibroblastic cells, this same C-terminal fragment was observed to decorate actin stress fiber-like structures and appeared to bring about their accumulation (Bartles *et al*., 1996). On the basis of its localization and actin-binding properties, we hypothesized that espin was an actin-bundling protein involved in cross-linking the actin filaments to form the bundles observed within the ES junctional plaque (Bartles *et al*., 1996). Additional evidence in support of this hypothesis came through our recent identification of a smaller (253-amino-acid) isoform of espin, "small espin," associated with the parallel actin bundles of brush border microvilli in the intestine and kidney (Bartles *et al*., 1998). Small espin was observed to bundle actin filaments in vitro under physiological conditions and displayed the properties of a third, albeit relatively minor, actin-bundling protein that, on the basis of its site of accumulation along the crypt–villus axis in adult intestine, would appear to act subsequently to villin and fimbrin/plastin during the assembly of brush border microvilli (Bartles *et al*., 1998).

Espin and small espin share an identical C-terminal 167-amino-acid peptide, which includes a 116-amino-acid peptide that we found could account for the in vitro actin-bundling activity of small espin in its entirety (Bartles *et al*., 1996, 1998). However, the two espin isoforms contain vastly different N termini. The N terminus of espin is relatively long and contains multiple motifs (eight ankyrin-like repeats and two proline-rich peptides) that, for other proteins, have been implicated in mediating protein–protein interactions (Bartles *et al*., 1996). In contrast, the N terminus of small espin contains two small unique peptides separated by another small peptide shared with espin (Bartles *et al*., 1998). In this article, we describe the basis for the differences in primary structure observed between espin and small espin, compare the actin-binding and -bundling properties of the two espin isoforms, and present the results of biochemical quantification and developmental immunolocalization experiments designed to test further our hypothesis that espin is a major actin-bundling protein of the ES junctional plaque.

MATERIALS AND METHODS

Sequencing of the Mouse Espin Gene

A genomic DNA clone that contained a portion of the mouse espin gene was obtained by screening a commerical strain 129/SvJ mouse genomic DNA library in the Lambda Fix II vector (Stratagene, La Jolla, CA) by Southern blotting using randomly primed ^{32}P-labeled rat espin cDNAs. The DNA was subjected to automated sequence analysis using Big Dye terminator and the model 377 sequencer (Applied Biosystems, Foster City, CA) and was found to contain multiple elements with a high degree of sequence similarity to the rat espin and small espin cDNAs (Bartles *et al*., 1996, 1998) (U46007 and AF076856). The BLAST program (Altschul *et al*., 1997) was used to optimize the alignment of these elements to derive a complete sequence of the mouse homologue of small espin and a partial sequence of the mouse homologue of espin. Putative exon–intron boundaries were selected by inspection and confirmed for the entire coding sequence of mouse small espin (and hence for those portions of mouse espin shared with mouse small espin) either by consulting the mouse Expressed Sequence Tag database (AA139619 and AU022485) or by sequencing the products (AF134857) obtained by PCR analysis of a commercial mouse testis cDNA library (Clontech, Palo Alto, CA).

Expression and Purification of Recombinant Proteins

For the expression of recombinant proteins, cDNAs were introduced into the pProEX HT prokaryotic expression vector (Life Technologies, Gaithersburg, MD) that gave the proper reading frame. N- or C-terminally truncated versions of espin were prepared using selected restriction enzyme fragments. The resulting pProEX HT constructs were checked by automated DNA sequencing and used to transform *Escherichia coli* DH5α (Life Technologies) or BL21 (Amersham Pharmacia Biotech, Piscataway, NJ). The recombinant proteins included an additional 28 amino acids at their N terminus: MSYY, followed by HHHHHH (the 6xHis tag), DYDIPTT (a spacer region), ENLYFQ (tobacco etch virus protease cleavage site) and GAMGS. The C-terminally truncated proteins also contained up to

15 additional amino acids at their C terminus, which were derived from the sequence of the polylinker before the built-in stop codons in the vectors. 6xHis-tagged espin constructs were isolated from 50 mM Tris-HCl, 10 mM 2-mercaptoethanol, pH 8.5, extracts of frozen and thawed, sonicated bacteria by batch affinity chromatography on Ni-nitrilotriacetic acid (NTA) agarose (Qiagen, Santa Clarita, CA) using the 0.1 M KCl, 10% (vol/vol) glycerol, 10 mM 2-mercaptoethanol, 20 mM Tris-HCl, 20 mM imidazole-HCl, pH 8.5, nondenaturing buffer system recommended by Life Technologies. Isolation of full-length recombinant espin required the addition of 0.3% (wt/vol) *N*-lauroylsarcosine just before sonication and 1% (vol/vol) Triton X-100 immediately after sonication. For all recombinant proteins except full-length espin, the 0.2 M imidazole eluate was dialyzed overnight at 4°C against 0.1 M KCl, 10 mM imidazole-HCl, 1 mM dithiothreitol, 1 mM NaN_3, pH 7.4, and freed of any insoluble protein by centrifugation at 150,000 × *g* for 90 min at 4°C in preparation for use in F-actin-binding and -bundling assays. For full-length espin, the 0.2 M imidazole eluate was maintained at 4°C and used in the actin-bundling assays immediately after centrifugation at 150,000 × *g* for 90 min. In some experiments, the 6xHis tag was removed from a recombinant protein by treating the dialyzed protein at a concentration of 0.02–0.05 mg/ml with 15 U/ml recombinant 6xHis-tagged tobacco etch virus protease (Life Technologies) for 3 h at 37°C and then incubated for 30 min at 4°C with Ni-NTA agarose to remove cleaved 6xHis-tag, any uncleaved 6xHis-tagged espin protein, and the residual 6xHis-tagged viral protease.

Actin-binding and -bundling Assays

F-actin was prepared by dilution of purified rabbit skeletal muscle actin (Cytoskeleton, Denver, CO) into 0.1 M KCl, 2 mM $MgCl_2$, 1 mM ATP, 1 mM NaN_3, 10 mM imidazole-HCl, pH 7.4, and incubation for 60 min at 37°C. To assay for F-actin binding or bundling, an equal volume of solution containing different amounts of recombinant espin protein (see above) was added to the preformed actin filaments (at a final actin concentration of 0.1–0.5 mg/ml) and incubated for 60 min at 37°C. Samples were then taken for negative staining with 1% (wt/vol) uranyl actetate on 300-mesh Formvar- and carbon-coated copper grids (Cooper and Pollard, 1982; Bartles *et al.*, 1998) or were centrifuged at 4°C for either 15 min at 22,000 × *g* (bundling assay; Edwards *et al.*, 1995; Bartles *et al.*, 1998) or for 90 min at 150,000 × *g* (binding assay; Bartles *et al.*, 1996, 1998), and the levels of espin protein and actin present in the supernatant and pellet were determined by scanning laser densitometric analysis of Coomassie blue-stained SDS gels using rabbit skeletal muscle actin as the protein standard. Data from densitometry scans were analyzed by the Microcal Origin 3.78 software available through the Keck Biophysics Facility at Northwestern University, and the dissociation constants and the numbers of binding sites on the actin filaments for the different espin constructs (with their SEs) were calculated by nonlinear least-squares-fitting plots of bound versus free to a rectangular hyperbola.

Sedimentation Equilibrium

For sedimentation equilibrium, the purifed recombinant ΔN338-espin was dialyzed against 0.1 M KCl, 0.02 M Tris-HCl, 5 mM 2-mercaptoethanol, 1 mM $MgCl_2$, 1 mM NaN_3, pH 7.4, freed of any insoluble protein by centrifugation at 150,000 × *g* for 90 min at 4°C, and centrifuged at 4°C for 24 h at 12,000 rpm and then for 30 h at 17,000 rpm in a Beckman Instruments (Palo Alto, CA) XL-A 70 analytical ultracentrifuge, collecting scans of A_{280} at 6-h intervals. The data were analyzed using the Beckman XL-A-Ultrascan-Microcal Origin 3.78 software supplied with the instrument, and subunit molecular masses were calculated by nonlinear least-squares-fitting plots of A_{280} versus (radius squared)/2 at equilibrium to an exponential curve using the Nonlin version 1.060 (D.A. Yphantis, M.L. Johnson, and J.W. Lary) and Sednterp version 1.00 (D.B. Hayes, T. Laue, and J. Philo) software available through the Keck Biophysics Facility at Northwestern University and on the Internet (www.cauma.uthscsa.edu/software).

Transient Transfection

For transient transfection, a cDNA encoding the designated espin construct was introduced into the pEGFP-C vector (Clontech) that gave the proper reading frame. The construct was checked by automated DNA sequencing and used to express a green fluorescent protein (GFP) fusion protein in cells of the baby hamster kidney (BHK) fibroblastic line (American Type Culture Collection, Manassas, VA) by transient transfection with LipofectAMINE (Life Technologies). The cells were cultured on coverslips in Dulbecco's modified Eagle's medium containing 10% (vol/vol) calf serum and penicillin-streptomycin. Eighteen to 24 h after transfection, the GFP-espin fusion protein was localized by conventional fluorescence microscopy, either without fixation or after fixation with 2% paraformaldehyde in PBS, extraction for 1 min with ice-cold 0.1% (vol/vol) Triton X-100 in PBS, and labeling with rhodamine-phalloidin (Molecular Probes, Eugene, OR). To control for the effects of GFP, selected espin constructs were expressed without GFP, using the pcDNA3 expression vector (Invitrogen, San Diego, CA), and detected by immunofluorescence (Bartles *et al.*, 1996).

Quantification and Extraction

Late spermatids were isolated from gently minced, decapsulated rat testes by centrifugation in a gradient of Percoll (Petruszak *et al.*, 1991; Bartles *et al.*, 1996). A vast majority of the late spermatids isolated in this way retain an ES, including the junctional plaque, as a tightly adherent fragment of Sertoli cell plasma membrane attached to their head (Bartles *et al.*, 1996). To determine the amount of espin or actin present in the ES, samples containing known numbers of these late spermatid–ES complexes, as determined using a hemocytometer, were compared with internal standards containing different amounts of recombinant espin (see above) or rat testicular actin-myosin (courtesy of Dr. Christine Collins, Abbott Laboratories, North Chicago, IL; and Dr. Ameet Kini, Northwestern University Medical School) by scanning laser densitometric analysis of Western blot autoradiograms. The number of espin or actin molecules present in the fraction was determined by comparison to the corresponding standard curve. Espin was detected using affinity-purified rabbit polyclonal antibodies directed against the C-terminal 379-amino-acid peptide of rat espin followed by ^{125}I-protein A (Bartles *et al.*, 1996), and actin was detected using the C4 monoclonal antibody (Chemicon International, Temecula, CA), which reportedly reacts with all nonmuscle and muscle vertebrate isoactins (Lessard, 1988; Sawtell and Lessard, 1989), followed by ^{125}I-goat anti-mouse immunoglobulin G (Jackson ImmunoResearch, West Grove, PA) (Bartles *et al.*, 1996). In some cases, the isolated late spermatid–ES complexes were extracted for 45 min with either 1% (vol/vol) Triton X-100 or 0.6 M KI at 4°C or with 7 M urea or 1% SDS at room temperature, all in PBS, pH 7.4, containing a mixture of protease inhibitors (Bartles *et al.*, 1998), before being centrifuged for 45 min at 150,000 × *g* and used to prepare supernatant and pellet fractions for Western blot analysis.

Immunoperoxidase Cytochemistry and Electron Microscopy

Immunoperoxidase labeling was carried out as described in detail by Cesario *et al.* (1995). Briefly, rat testis was fixed by perfusion through the abdominal aorta with Bouin's fluid and embedded in paraffin. Five-micrometer sections were deparaffinized with xylenes, labeled with affinity-purified rabbit polyclonal espin antibody or preimmune immunoglobulin G followed by horseradish peroxidase-conjugated donkey anti-rabbit F(ab')$_2$, reacted with H_2O_2 and 3,3′-diaminobenzidine, and counterstained with hematoxylin. The assignment of semininferous tubules to different stages of the cycle

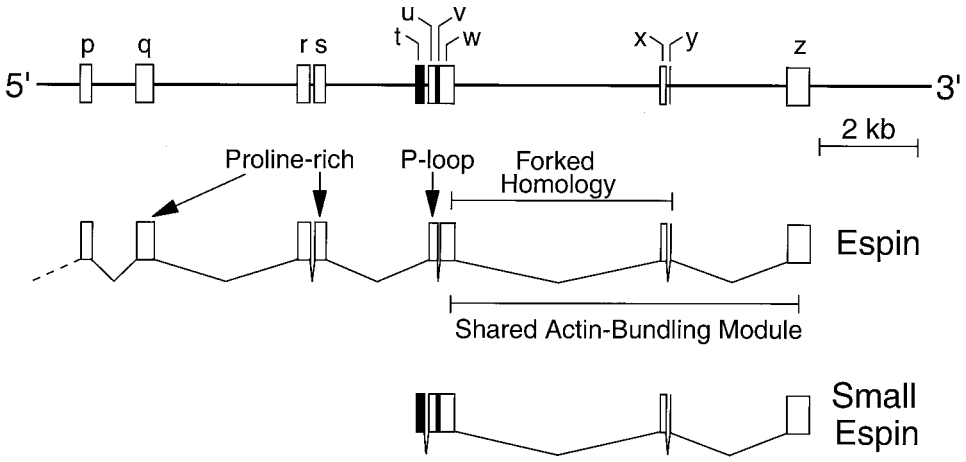

Figure 2. Organization of the mouse espin gene. This diagram depicts the relative sizes and positions of the exons deployed differentially to construct small espin and approximately the C-terminal 60% of espin in the mouse. It highlights the positions of the exons that encode the two proline-rich peptides, the potential P-loop, the 66-amino-acid forked homology domain, and the shared C-terminal actin-bundling module (Bartles *et al.*, 1996, 1998). The shaded exons, t and v, are specific to small espin. These sequence data are available from GenBank under accession number AF134858.

of the seminiferous epithelium (Leblond and Clermont, 1952a) and of spermatids to the different steps of spermiogenesis (Leblond and Clermont, 1952b) was carried out at the light microscopic level through the analysis of hematoxylin- or toluidine blue-counterstained sections using the criteria outlined in detail by Russell *et al.* (1990). For transmission electron microscopy, rat testis was fixed by perfusion through the abdominal aorta with 1.5% paraformaldehyde, 1.5% glutaraldehyde in 0.1 M sodium cacodylate, pH 7.3, after a brief clearing with Ringer's solution containing 0.1% (wt/vol) each of procaine and sodium nitroprusside (Cesario *et al.*, 1995). The tissue was cut into small pieces, and the pieces were postfixed for 2 h in the same fixative and for 1 h in 1% OsO_4, stained en bloc with 1% uranyl acetate for 1 h at room temperature, dehydrated through a graded series of ethanol solutions and propylene oxide, and embedded in PolyBed 812 (Polysciences, Warrington, PA). Semithin sections were stained with toluidine blue and examined to identify tubules containing spermatids in the different steps of spermiogenesis. Block faces were then trimmed to isolate a given tubule for the preparation of ultrathin sections, which were examined after staining with uranyl acetate and lead citrate.

RESULTS

Organization of the Espin Gene

An 18,015-bp genomic DNA clone obtained by library screening was used to derive a complete sequence of the mouse homologue of small espin and a partial sequence of the mouse homologue of espin (GenBank accession number AF134858). The genomic fragment contained 11 recognizable exons, which we provisionally named p–z, distributed over ~15 kb (Figure 2). The complete coding sequence and 3′-untranslated sequence of mouse small espin could be accounted for by linking together exons t–z (Figure 2). A partial sequence of mouse espin that included most of the protein, with the exception of its eight N-terminal ankyrin-like repeats, could be accounted for by linking exons p–s, u, and w–z (Figure 2). The amino acid sequences predicted for mouse small espin and this portion of mouse espin were found to be ~95% identical to their counterparts in the rat. One hundred percent amino acid sequence identity was noted for exons s, u, and x–z, which encode, respectively, the second of the two proline-rich peptides that are present in espin but not in small espin, the potential P-loop shared by espin and small espin, and much of the C-terminal actin-bundling module that is shared between espin and small espin (Figure 2; Bartles *et al.*, 1998). These sequence data support the hypothesis that espin and small espin arise through differential splicing of the primary transcript obtained from a single espin gene. Southern blot tests for gene multiplicity, using multiple espin cDNA probes and restriction enzymes, also supported the hypothesis that there is a single espin gene in both the mouse and the rat (our unpublished data).

Actin Binding and Bundling by Recombinant Espin

To examine the actin-binding and -bundling properties of espin, the full-length protein was expressed with an N-terminal 6xHis-tag in *E. coli*. The 6xHis-tagged full-length espin proved to be insoluble when the bacteria were lysed using our standard nondenaturing conditions (Bartles *et al.*, 1998). It could, however, be solubilized sufficiently to allow for affinity purification by adding 0.3% *N*-lauroylsarcosine before sonication and 1% Triton X-100 immediately after sonication. Although soluble upon elution from the Ni-NTA agarose, the full-length espin gradually precipitated if the temperature was raised above 8–10°C and/or if the buffer composition was changed to more physiological conditions by dialysis. Nevertheless, when mixed with preformed filaments of rabbit skeletal muscle actin at ratios of ~1 espin for every 10–15 actin monomers and maintained at 4–8°C for 1 h in a buffer more similar to that used in protein purification (final concentrations, 0.1 M KCl, 0.1 M imidazole-HCl, 5 mM 2-mercaptoethanol, 1 mM $MgCl_2$, 0.5 mM ATP, 1 mM NaN_3, pH 8.5), the 6xHis-tagged full-length espin was observed to bundle the actin filaments efficiently. The bundling was evident as an increase in solution turbidity (our unpublished data), a shift of the majority of the F-actin (and espin) from the supernatant to the pellet in the low-speed centrifugation actin-bundling assay (Figure 3, left panel) and by negative staining electron microscopy (Figure 4C).

The insolubility of the recombinant full-length protein appeared to be due to the peptide that contains the eight ankyrin-like repeats and constitutes approximately the N-terminal third of espin. When expressed in *E. coli* with an N-terminal 6xHis-tag, the ankyrin repeat portion of espin was completely insoluble in the absence of protein denaturants (our unpublished data). In contrast, a 6xHis-tagged

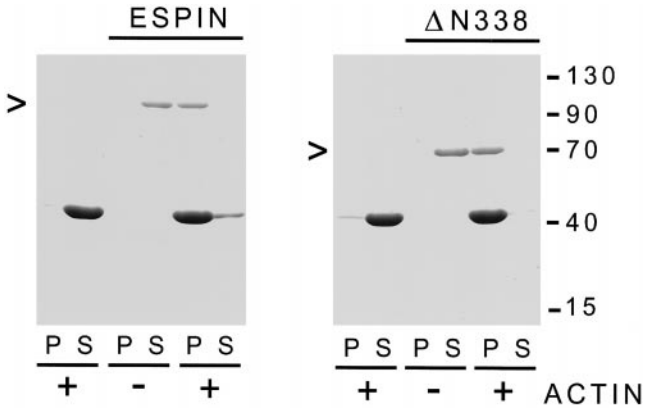

Figure 3. Actin binding and bundling by recombinant espin and ΔN338-espin as revealed by the low-speed centrifugation assay. Shown are Coomassie blue-stained gels of the pellet (P) and supernatant (S) that result from low-speed centrifugation when rabbit skeletal muscle F-actin was incubated alone or in the presence of either recombinant full-length espin for 1 h at 4°C in 0.1 M KCl, 0.1 M imidazole-HCl, 5 mM 2-mercaptoethanol, 1 mM $MgCl_2$, 0.5 mM ATP, 1 mM NaN_3, pH 8.5 (left panel), or recombinant ΔN338-espin for 1 h at 37°C in 0.1 M KCl, 10 mM imidazole-HCl, 0.5 mM dithiothreitol, 1 mM $MgCl_2$, 0.5 mM ATP, 1 mM NaN_3, pH 7.4 (right panel). The arrowheads at the left denote the position of the recombinant espin construct. The actin is the major band migrating slightly above the 40-kDa marker.

ΔN338 deletion construct of espin, which was missing the ankyrin-like repeat peptide, was found to be completely soluble in bacterial lysates, thereby allowing its isolation using our standard nondenaturing conditions. Furthermore, the purified recombinant ΔN338-espin retained its solubility under a variety of conditions, so that it could be assayed for actin-binding and -bundling activities under our standard physiological buffer conditions at 37°C. Because of this advantage, we decided to concentrate on an examination of the actin-binding and -bundling properties of the ΔN338 construct. Full-length espin and ΔN338-espin were indistinguishable in their localizations and effects on the actin cytoskeleton when expressed ectopically as GFP fusion proteins in transiently transfected BHK fibroblastic cells. Both proteins were observed to decorate fine to coarse stress fiber-like structures in the living cells. Examples of cells expressing GFP-espin are shown in Figure 5, A and B. As observed previously for BHK cells expressing GFP-small espin (Bartles *et al.*, 1998), upon fixation and permeabilization and double labeling with rhodamine-phalloidin, the espin-containing stress fiber-like structures showed an accumulation of F-actin (our unpublished data). Similar results were obtained when the proteins were expressed without the GFP moiety and localized by immunofluorescence (our unpublished data).

When incubated with rabbit skeletal muscle F-actin for 1 h at 37°C under our standard physiological buffer conditions (final concentrations, 0.1 M KCl, 10 mM imidazole-HCl, 0.5 mM dithiothreitol, 1 mM $MgCl_2$, 0.5 mM ATP, 1 mM NaN_3, pH 7.4), ΔN338-espin was found to bind to F-actin with high

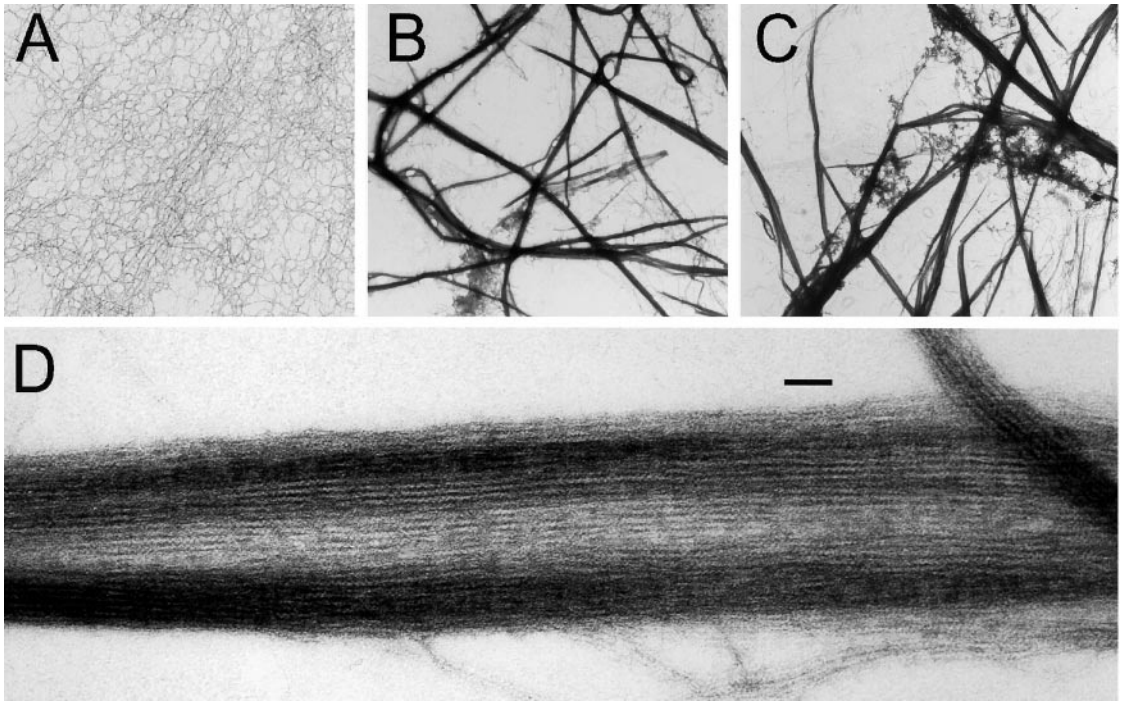

Figure 4. Actin bundling by recombinant espin and ΔN338-espin as revealed by negative staining. Rabbit skeletal muscle actin was incubated alone (A) or in the presence of recombinant full-length espin (C) or recombinant ΔN338-espin (B and D) under the conditions of Figure 3, and aliquots were taken for negative staining. (A–C) Low magnification (bar in D, 770 nm); (D) high magnification (bar, 37 nm).

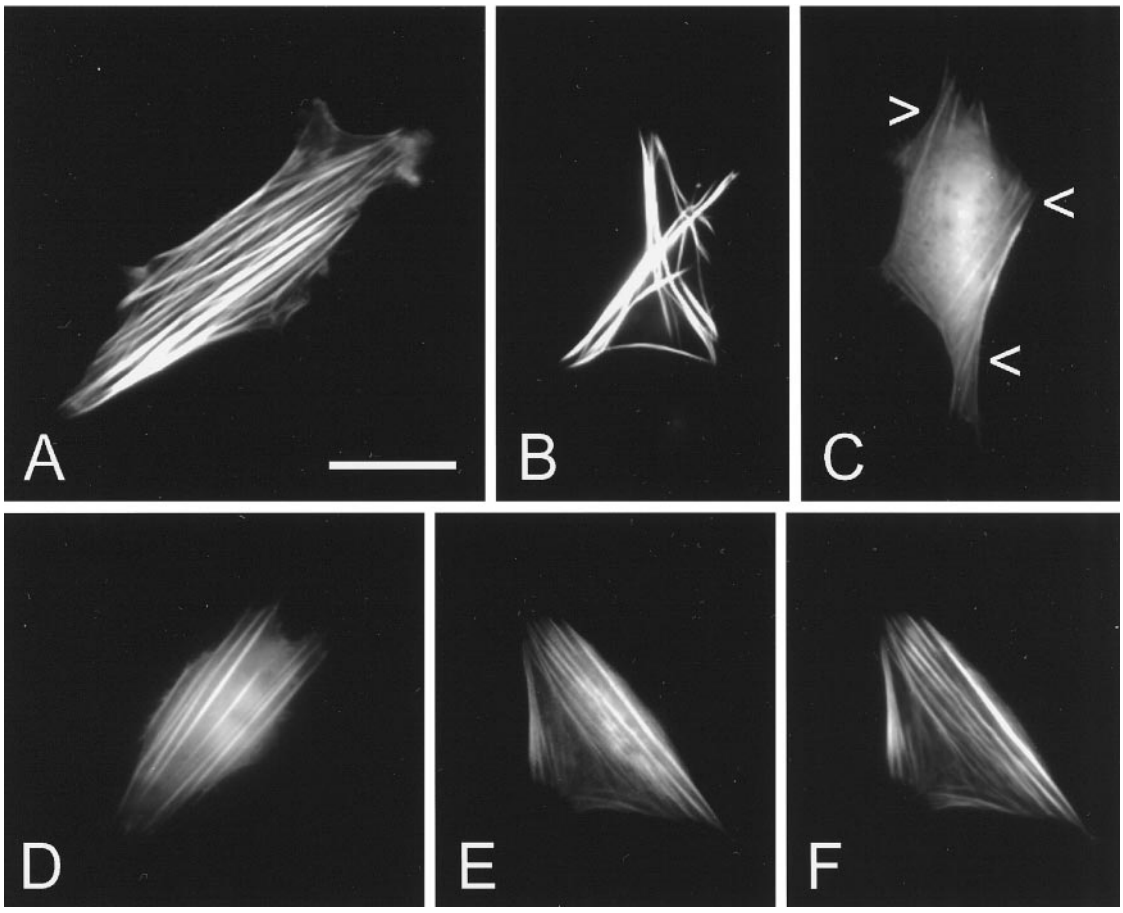

Figure 5. Localization of GFP-espin and GFP-espin(339–720) in transiently transfected BHK cells. (A and B) GFP-espin in living cells. (C and D) GFP-espin(339–720) in living cells. Arrowheads in C denote fine labeled filaments observed in the thinner parts of cell near the periphery. (E and F) GFP-espin(339–720) (E) and rhodamine-phalloidin (F) in fixed and permeabilized cell. Bar in A, 25 μm.

affinity. When the binding data were fit to a rectangular hyperbola, the K_d was calculated to be 70 ± 10 nM, and the number of binding sites on the actin filaments for ΔN338-espin was calculated to be 0.27 ± 0.01 espin per actin monomer (R^2 = 0.97; Figure 6A). When reanalyzed using the same fitting procedure, the published data for the binding of small espin to rabbit skeletal muscle F-actin (Bartles *et al*., 1998) gave a K_d of 220 ± 50 nM (R^2 = 0.99), suggesting that ΔN338-espin bound to rabbit skeletal muscle F-actin with a 3.2-fold higher affinity than small espin. ΔN338-espin also proved to bundle actin filaments efficiently, as revealed by solution turbidity (our unpublished data), the low-speed centrifugation actin-bundling assay (Figure 3, right panel), and negative staining (Figure 4B). Consistent with its higher affinity for binding to F-actin, the ΔN338-espin appeared to be ~2.5-fold more efficient, on a molar basis, than small espin at causing the shift of F-actin from the supernatant to the pellet in the low-speed centrifugation actin-bundling assay (Figure 6B). When examined by negative staining electron microscopy at higher magnification, the actin bundles elicited by ΔN338-espin (Figure 4, B and D) and full-length espin (our unpublished data) resembled those formed by small espin (Bartles *et al*., 1998). The bundles showed the regular close packing and axial alignment of filaments typical of parallel actin bundles (DeRosier and Tilney, 1981; Stokes and DeRosier, 1991). In addition, the bundles appeared to be partially ordered, displaying regions where the transverse banding pattern at ~37-nm intervals indicative of paracrystalline order within an actin bundle (DeRosier and Tilney, 1981; Stokes and DeRosier, 1991) could be recognized, but these regions generally appeared to be aligned imperfectly across the width of the bundle (Figure 4D). As was the case for small espin (Bartles *et al*., 1998), the actin-bundling activity of ΔN338-espin was unaffected by exogenous Ca^{2+} (concentrations of 1 μM to 1 mM) or chelating agents (1 mM EDTA) and was observed with or without prior removal of the N-terminal 6xHis-tag with tobacco etch virus protease (our unpublished data).

Sedimentation Equilibrium Analysis and Actin Binding by Espin Constructs Missing the Shared C-terminal Actin-bundling Module

The increased F-actin-binding affinity of ΔN338-espin compared with small espin appeared not to be due to a difference in oligomeric state; sedimentation equilibrium analysis showed that ΔN338-espin was also a monomer in solution,

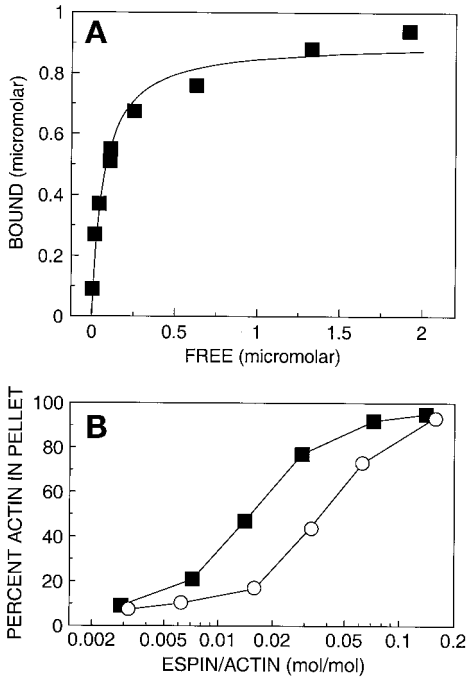

Figure 6. Concentration dependence of actin-binding and -bundling by recombinant ΔN338-espin. (A) Direct plot of bound versus free for the binding of different concentrations of recombinant ΔN338-espin to a fixed concentration of rabbit skeletal muscle F-actin using the high-speed centrifugation actin-binding assay under the conditions of Figure 3, right panel. The curve was obtained by nonlinear least-squares fitting to a rectangular hyperbola. (B) Percent of actin obtained in the pellet in the low-speed-centrifugation actin-bundling assay as increasing concentrations of recombinant ΔN338-espin (solid squares) or recombinant small espin (open circles) were added to a fixed concentration of F-actin.

at and above the concentrations that caused efficient bundling in vitro. The sedimentation equilibrium data for ΔN338-espin were best fit by assuming a single sedimenting species with a molecular mass of 53 ± 5 kDa (mean ± SD; n = 4), i.e., only ~8% less than the value of 57.5 kDa expected for a monomer on the basis of predicted amino acid sequence. Instead, it appeared that the increased binding affinity was due to the presence of an additional actin-binding site in the N terminus of espin. A deletion construct of ΔN338-espin, espin(339–720), which was missing the 116-amino-acid C-terminal actin-bundling module, was found to bind to F-actin in vitro (Figure 7, A and B) and apparently also in transfected cells (see below). When the binding data were fit to a rectangular hyperbola, the K_d was calculated to be 1.0 ± 0.2 μM, and the number of binding sites on the actin filaments for espin(339–720) was calculated to be 0.23 ± 0.03 espin per actin monomer (R^2 = 0.98; Figure 7B). Consistent with its lower affinity for binding to F-actin in vitro, there was a larger pool of cytoplasmic and nuclear–perinuclear labeling observed for GFP-espin(339–720) in transfected BHK cells than for any of the GFP-tagged constructs that contained the shared C-terminal actin-bundling module (Figure 5, compare C and D with A and B). Nonetheless, it was frequently possible to discern a fine stress fiber-like pattern of labeling superimposed on this relatively high cytoplasmic background, especially at the relatively thin margins of well-spread cells (Figure 5C, arrowheads). Occasionally, the stress fiber-like structures labeled by GFP-espin(339–720) were more prominent (Figure 5D). No labeled stress fiber-like structures were observed when the BHK cells were made to express GFP alone, in the absence of espin fragment (Bartles *et al.*, 1998; our unpublished data). When the cells were fixed, permeabilized, and double labeled with rhodamine-phalloidin, it was apparent that the GFP-espin(339–720)-containing stress fiber-like structures colocalized with F-actin (Figure 5, E and F). These data suggested that espin(339–720) also bound to F-actin in vivo.

To map the actin-binding site of espin(339–720), we examined the in vitro actin-binding activities of several other 6xHis-tagged deletion constructs (Figure 7C). Peptides immediately adjacent to the shared C-terminal actin-bundling module, e.g., espin(564–720), did not bind to F-actin, whereas those derived from a more N-terminal location displayed saturable binding (Figure 7C). The smallest constructs examined that displayed saturable binding were espin(396–481) and espin(459–542). These data suggested that a peptide necessary for the activity the additional actin-binding site was present in the region of overlap between these two small constructs, i.e., in a 23-amino-acid peptide just C-terminal to the N-terminal proline-rich peptide (Figure 7C). Espin(459–542) was also tested for its interactions with the actin cytoskeleton in vivo when expressed as a GFP fusion protein in transfected BHK cells. Like GFP-espin(339–720) (Figure 5, C–F), GFP-espin(459–542) was found to decorate actin stress fiber-like structures (our unpublished data).

Quantification and Extraction of ES-associated Espin

To quantify the number of molecules of espin associated with the ES, we enriched those cells released from gently minced testis for late spermatids by centrifugation in gradients of Percoll. Late spermatids prepared in this way frequently retain an ES, including the junctional plaque, tightly adherent to their head (Figure 1, right; Bartles *et al.*, 1996). 90–95% of the cells recovered in the procedure were judged to be late spermatids on the basis of morphology (the remainder being unidentified round cells and erythrocytes), and 90–95% of the late spermatids were judged to be complexed to an ES junctional plaque on the basis of intense immunofluorescent labeling of phase-dense material surrounding the head using the espin antibody (Bartles *et al.*, 1996). None of the other cells in the preparation showed significant labeling with the espin antibody. Samples containing known numbers of these late spermatid–ES complexes were compared with internal standards containing different amounts of recombinant espin on Western blots, and the number of espin molecules per isolated late spermatid–ES complex was estimated to be 4–5 × 10^6 (range of two independent determinations). When compared with internal standards of rat testicular actin on Western blots using the C4 monoclonal actin antibody, the number of actin monomers associated with the late spermatid–ES complex in these two preparations was estimated to be 8–10 × 10^7 (range of two independent determinations). Therefore, the molar ratio of espin to actin monomer in the isolated late

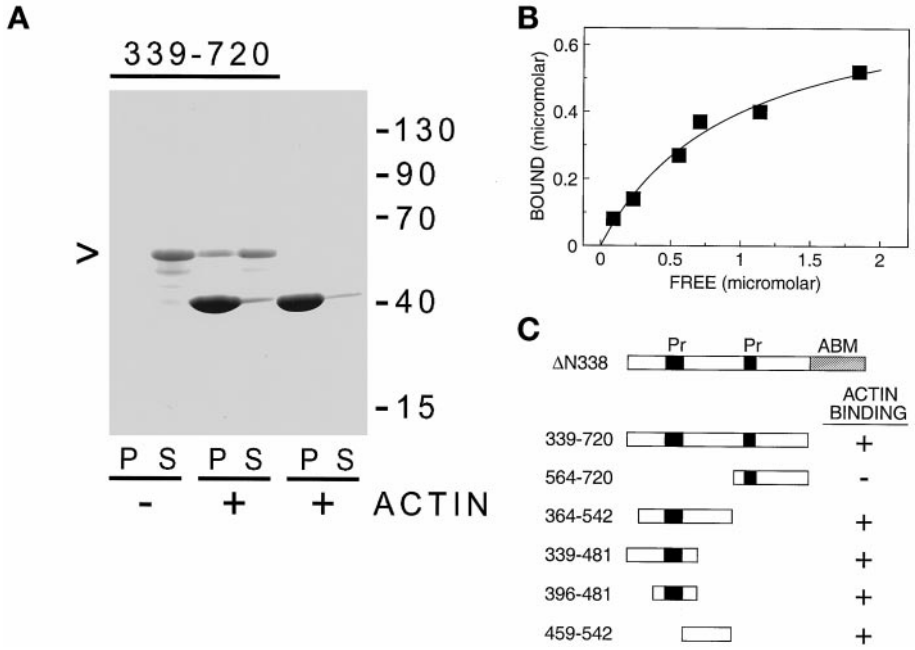

Figure 7. Actin binding by recombinant espin(339–720), a fragment from the N terminus of espin that is missing the C-terminal actin-bundling module, and the mapping of its actin-binding site by deletion mutagenesis. (A) Coomassie blue-stained gel of the pellet (P) and supernatant (S) that result from high-speed centrifugation when rabbit skeletal muscle F-actin is incubated alone or in the presence of recombinant espin(339–720) for 1 h at 37°C in 0.1 M KCl, 10 mM imidazole-HCl, 0.5 mM dithiothreitol, 1 mM $MgCl_2$, 0.5 mM ATP, 1 mM NaN_3, pH 7.4. The arrowhead at the left denotes the position of the recombinant espin construct. The actin is the major band migrating slightly above the 40-kDa marker. (B) Direct plot of bound versus free for the binding of different concentrations of recombinant espin(339–720) to a fixed concentration of rabbit skeletal muscle F-actin under the conditions of A. The curve was obtained by nonlinear least-squares fitting to a rectangular hyperbola. (C) Actin-binding activity of N- or C-terminal deletion constructs of espin(339–720). + or −, presence or absence of saturable actin-binding activity for the designated construct as determined by scanning laser densitometric analysis of the SDS gels that resulted from the high-speed centrifugation actin-binding assay (e.g., see A and B). In the accompanying diagrams, the two proline-rich peptides (Pr) are shaded, and the shared C-terminal actin-bundling module (ABM) present in the ΔN338-espin bar at the top is shown with fine diagonal hatching.

spermatid–ES complex was calculated to be ~1:20. Technically, this ratio could be even higher than ~1:20, because a portion of the actin present in the isolated late spermatid–ES complex is likely to come from the spermatid. Oko *et al.* (1991) have shown that when rat testis sections are labeled with the C4 monoclonal antibody, the antibody reacts most strongly with the ESs, but there is also some weak labeling of spermatids. Consistent with a tight association between espin and the actin cytoskeleton of the ES, the majority (75–80%) of the espin associated with the isolated late spermatid–ES complex resisted extraction with 1% Triton X-100 or 0.6 M KI for 45 min at 4°C. Harsher treatments, such as 7 M urea or 1% SDS at room temperature, were required to solubilize a higher percentage of the espin from the isolated late spermatid–ES complex (our unpublished data).

Time Course of Espin Accumulation during Spermiogenesis

Our previous immunoperoxidase immunocytochemical study examining paraffin sections of testis indicated that espin was concentrated around the head of the spermatid from mid through late spermiogenesis (Bartles *et al.*, 1996). For example, the spermatids shown in Figure 8A, which are in step 12 of the 19 commonly recognized steps of spermiogenesis (Leblond and Clermont, 1952b; Russell *et al.*, 1990), show an accumulation of brown immunoperoxidase reaction product around their elongated heads. Some immunoperoxidase reaction product can also be detected in an occasional wavy line near the base of the tubule. The latter presumably represents espin in the ES components of the Sertoli cell–Sertoli cell junctional complexes (Russell and Peterson, 1985; Vogl, 1989; Vogl *et al.*, 1991), and its intensity appears to vary during the cycle of the seminiferous epithelium (Bartles *et al.*, 1996; see other panels of Figure 8).

To determine more precisely when espin first accumulated in the vicinity of the head of the developing spermatid in relation to the time when actin bundles are known to first appear in the ES junctional plaque, we focused on spermatids in steps 7 and 8 of spermiogenesis. The actin bundles of the ES are not present in significant numbers beneath the Sertoli cell plasma membranes at surfaces in contact with rat spermatids in step 7 of spermiogenesis (Russell *et al.*, 1988; Renato de Franca *et al.*, 1993). They are first noted in early step 8, shortly after the acrosome–nucleus complex becomes closely apposed to the spermatid plasma membrane at one pole of the cell (Russell *et al.*, 1988; Renato de Franca *et al.*, 1993). The results of our electron microscopic analyses of ES formation agreed with those of the earlier studies of Renato de Franca *et al.* (1993) and Russell *et al.* (1988), and in Figure 9 we show an example of a region of close contact between a Sertoli cell and an early step 8 spermatid, which demonstrates that the layers that characterize the ES ultrastructurally are present. There is apparently a relatively rapid accumulation of parallel actin bundles during early step 8, because by late step 8 virtually all of the region of adjacent to the spermatid's acrosome has a recognizable ES with actin bundles (Russell *et al.*, 1988; Renato de Franca *et al.*, 1993; our unpublished data).

As spermatids like those depicted in Figure 8A continue their differentiation, they undergo a net movement in the direction of the tubule lumen. Figure 8B shows an example

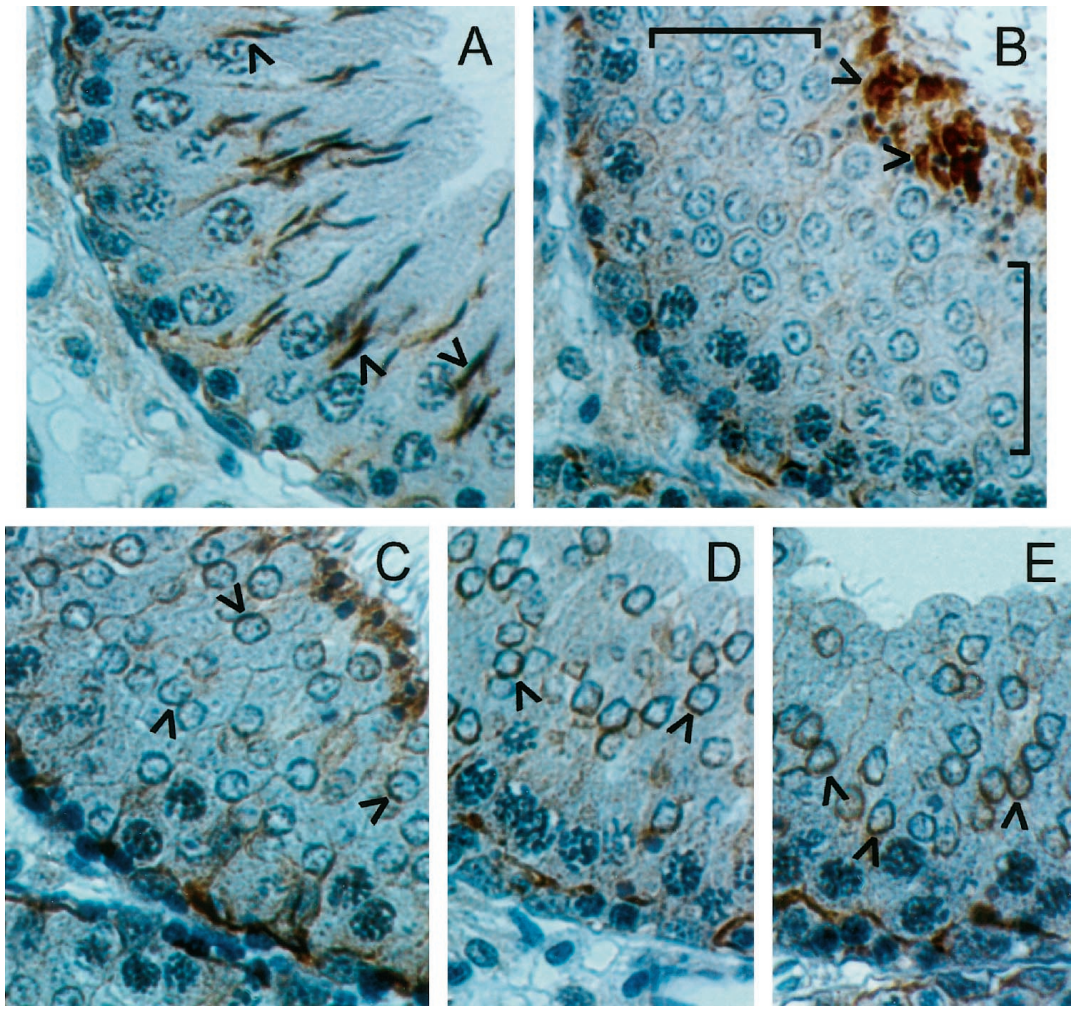

Figure 8. Immunoperoxidase localization of espin during spermiogenesis. Included are portions of cross-sectional profiles of seminiferous tubules containing spermatids in selected steps of spermiogenesis. In each case, the full span of the seminiferous epithelium is shown, from base (lower and/or left side of the panel) to lumen (upper and/or right side of the panel, where letter is shown). Arrowheads point to examples of areas where the brown immunoperoxidase reaction product indicative of espin can be detected at the site of the ES, i.e., near the heads of spermatids, in step 12 (A), step 19 (B), early step 8 (C), or late step 8 (D and E) of spermiogenesis. Spermatids in late step 7 of spermiogenesis, which do not show evidence of significant espin accumulation, occupy the central part of the seminiferous epithelium in B (zone delimited by brackets). Upper bracket in B, 60 μm.

of spermatids nearing the end of spermiogenesis. Note that these step 19 spermatids have become positioned so that their heads (arrowheads), which are labeled a deep brown and are clustered near the lumen, are for the most part even closer to the lumen than the dark blue dots that correspond to hematoxylin-stained RNA aggregates present within the cytoplasmic lobes of the spermatids (Russell *et al.*, 1990). During the period when the spermatids are moving in the direction of the lumen, a new wave of spermatids, derived from the division and differentiation of pachytene spermatocytes (cells with large ovoid nucleus just basal to the spermatids in Figure 8A), populates the central part of the epithelium (Figure 8B, area delineated by brackets). The spermatids depicted in the bracketed zone of Figure 8B are in late step 7 of spermiogenesis. Note that they still have their nucleus placed centrally, and that they show little or no immunoperoxidase labeling around their periphery. We examined 51, 78, and 57 independent profiles of seminiferous tubules containing spermatids in early, mid, and late step 7, respectively, in testis sections obtained from three rats, and in no case were higher amounts of labeling detected around the spermatid periphery. In contrast, spermatids in early step 8 (Figure 8C) and, especially, those in late step 8 (Figure 8, D and E) showed evidence of a significant concentration of espin at the site of the ES, i.e., as a C-shaped cap near the pole of the nucleus that was in contact with the edge of the spermatid (arrowheads). This pattern of labeling was observed for 93 and 39 independent profiles of seminiferous tubules containing spermatids we examined in early and late step 8, respectively. These data suggest that espin and the parallel actin bundles accumulate at approximately the same time, namely, during early step 8 of spermiogenesis.

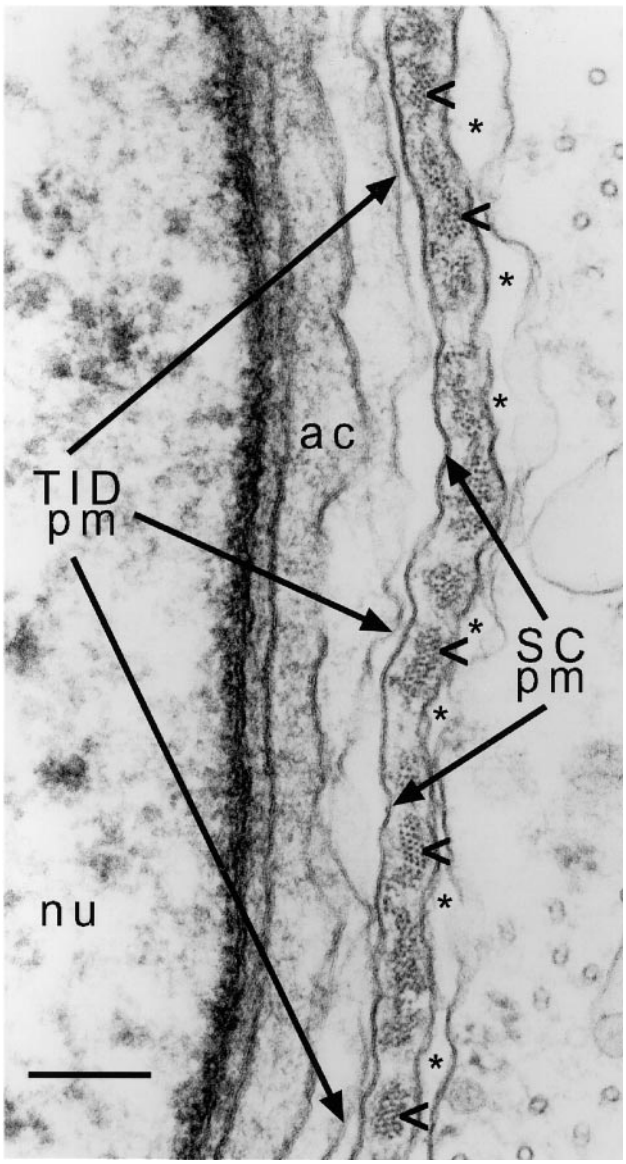

Figure 9. Electron micrograph highlighting the various layers of the ES and neighboring structures present at the site of contact between a Sertoli cell and an early step 8 spermatid in a section of rat testis. The right portion includes the Sertoli cell and highlights its plasma membrane (SC pm) and the parallel actin bundles (arrowheads) and cistern of endoplasmic reticulum (asterisks in lumen) that comprise the ES junctional plaque. Note that the parallel actin bundles are cut in cross section or near cross section, so that each actin filament appears as a small dot. The left portion includes the spermatid and highlights its plasma membrane (TID pm), nucleus (nu), and acrosome (ac). Bar, 0.18 μm.

Consistent with this conclusion, approximately one-half (42 of 93) of the seminiferous tubule profiles containing early step 8 spermatids showed a lower level of labeling or heterogeneous labeling, similar to that shown in Figure 8C, whereas the others (51 of 93) showed stronger and more uniform labeling, like that depicted in Figure 8, D and E. Note that the labeling observed at the luminal surface of the epithelium, which was very intense for the step 19 spermatids shown in Figure 8B, diminished in intensity, appearing to become localized to the apical cytoplasm of the Sertoli cell (Figure 8C), and then disappeared (Figure 8, D and E) around the time of sperm release. This change in localization presumably reflects the disassembly of the ES, which is believed to involve in part the transient formation of related structures known as tubulobulbar complexes (reviewed in Russell and Peterson, 1985; Vogl *et al.*, 1991).

DISCUSSION

On the basis of the following criteria, we conclude that espin is a major actin-bundling protein of the ES junctional plaque. Espin is localized to the parallel actin bundles of the ES junctional plaque in situ. The protein accumulates at the site of the ES coincident with the appearance of parallel actin bundles during spermiogenesis. Espin is present in 4–5 million copies per isolated late spermatid–ES complex, or at a ratio of at least ~1 espin for every 20 actin monomers, in a Triton X-100-insoluble cytoskeletal fraction. Recombinant espin and its selected fragments bind to F-actin with high affinity in vitro and efficiently cross-link the filaments into partially ordered bundles. When expressed ectopically in transiently transfected fibroblastic cells, espin and its selected fragments decorate actin stress fiber-like structures and appear to bring about their accumulation, presumably the result of filament bundling and/or stabilization. Finally, consistent with the molecular organization of other actin-bundling proteins (Matsudaira, 1991; Puius *et al.*, 1998), espin appears to be a monomer with multiple, in this case three, actin-binding sites. Although espin and small espin display a number of similarities and appear to be encoded by a single gene, we have uncovered some differences in their developmental regulation, stoichiometry, and interactions with F-actin that may ultimately help us understand why these two espin isoforms are restricted to particular cell types and parallel actin bundle-containing structures.

Our efforts to examine the in vitro actin-binding and -bundling properties of espin were hindered by the insolubility of the full-length protein when expressed in bacteria. Nevertheless, espin's tight association with ES junctional plaque and the consequences of ectopic overexpression on the actin cytoskeleton of transfected eukaryotic cells left us little choice but to concentrate on the bacterially expressed version of the protein. Fortunately, it was possible to overcome this insolubility problem to a large extent by solubilizing the full-length protein using *N*-lauroylsarcosine and Triton X-100 or through the examination of a construct that was missing the ankyrin repeats. Both approaches yielded proteins that were highly efficient at bundling F-actin in vitro. Although it remains a formal possibility that the ankyrin repeats could somehow influence interactions with F-actin, we think that the likelihood is small, given that 1) recombinant espin with its ankyrin repeats was able to bundle F-actin under conditions that were not too far from physiological; 2) we noted no difference in the effects of full-length espin and the ΔN338 derivative on the actin cytoskeleton of transfected BHK cells; and 3) multiple ankyrin repeats tend to form independently folded subdomains (Gay and Ntwasa, 1993; Michaely and Bennett, 1993, 1995).

Espin shows an affinity for binding to F-actin that is more than an order of magnitude greater than that displayed by other actin-bundling and cross-linking proteins and lateral actin filament-binding proteins (Bryan and Kane, 1978; Glenney *et al.*, 1981; Burgess *et al.*, 1987; Pollard, 1993). And, unlike some other actin-bundling proteins, such as fimbrin/plastin and villin (Glenney *et al.*, 1981; Alicea and Mooseker, 1988; Namba *et al.*, 1992; Lin *et al.*, 1994), espin binds to and bundles F-actin in a Ca^{2+}-insensitive manner in vitro. ΔN338-espin bound to F-actin with an affinity that was ~3-fold higher than small espin and was ~2.5-times more potent at eliciting bundle formation in vitro. Because both small espin and ΔN338-espin proved to be monomeric in solution, these differences are probably not attributable to differences in oligomeric state. Instead, our deletion mutagenesis of ΔN338-espin suggests that this difference could be due to the presence of an additional actin-binding site in the N terminus of espin that is not present in small espin. Given that espin presumably contains the two actin-binding sites inferred to be present within the shared C-terminal actin-bundling module on the basis of our previous deletion mutagenesis studies (Bartles *et al.*, 1998), this would bring the total number of actin-binding sites in espin to three.

The additional actin-binding site detected in the N terminus of espin appears to map to a 23-amino-acid peptide (amino acid residues 459–481) that is just C-terminal to the N-terminal proline-rich peptide and is included in the peptide encoded by exon q. On the basis of our analysis of the binding of espin(339–720), this additional actin-binding site appears to bind to F-actin with a K_d of ~ 1 μM. Although this affinity is ~4.5- and ~14-fold less than that observed for the binding of small espin and ΔN338-espin, respectively, it is important to point out that this fragment of espin, which is missing the C-terminal actin-bundling module, still binds to F-actin with an affinity that is comparable with that reported for the binding of other actin-bundling proteins, such as fascin, fimbrin/plastin, and villin (Bryan and Kane, 1978; Glenney *et al.*, 1981; Burgess *et al.*, 1987), and a large group of other actin-binding proteins (Pollard, 1993). The 23-amino-acid peptide in question, HLDNIYMQTKNKLRHVEVDSLKK, contains the hexapeptide LRHVEV that bears a partial resemblance to the LKHAET-like motif implicated by covalent cross-linking in the binding of the protein actobindin to actin and present in other actin-binding proteins (Vancompernolle *et al.*, 1991). In addition, this 23-amino-acid peptide contains clustered amino acids with positively charged side chains, which have been implicated in the actin-binding sites of other proteins (Yonezawa *et al.*, 1989; Yamamoto, 1991; Friederich *et al.*, 1999). But other than this, the peptide does not show any obvious resemblance to the actin-binding sites of other proteins. Our observation that GFP-espin(339–720) and GFP-espin(396–481), which contain the peptide of interest but are missing the shared C-terminal actin-bundling module, appear to decorate actin stress fiber-like structures in transfected cells suggests that this additional actin-binding site also functions in vivo. The reason for espin having an extra actin-binding site in its N terminus remains unclear, but an increase in the valency of the binding interaction between espin and F-actin would be expected to make a positive contribution to the stability of a bundle (Furukawa and Fechheimer, 1997) and possibly to the filaments as well (Zigmond *et al.*, 1992). It is also presently unclear whether the additional actin-binding site might compete with, or otherwise influence, the actin-binding sites of espin's C-terminal actin-bundling module and whether the additional actin-binding site would attach to one of the same filaments as the C-terminal actin-bundling module or to a different filament.

Espin also differed from small espin in its stoichiometry and developmental regulation. Small espin appears to be a relatively minor protein of brush border microvilli, being detected at a ratio of only ~1 small espin for every 130 actin monomers in brush borders isolated from rat small intestine (Bartles *et al.*, 1998). In contrast, espin was detected in 4–5 × 10^6 copies per late spermatid–ES complex, which translates into a ratio of at least ~1 espin for every 20 actin monomers. Small espin appears to accumulate relatively late during the process of brush border microvillus assembly (Bartles *et al.*, 1998), significantly later than when the microvillar actin bundles and the two major actin-bundling proteins, villin and fimbrin/plastin, accumulate within the brush border (Ezzell *et al.*, 1989; Heintzelman and Mooseker, 1992; Fath and Burgess, 1995). In constrast, espin appears to accumulate at the site of the ES coincident with the accumulation of the parallel actin bundles during spermiogenesis. More specifically, of the ~22 d required to complete spermiogenesis in the rat, espin and the parallel actin bundles accumulate at the site of the ES during the same ~15-h window that encompasses early step 8 of spermiogenesis (for durations of the different steps, see Russell *et al.*, 1990). Therefore, unlike the situation for small espin, which appears to be added in relatively small numbers to an already largely assembled parallel actin bundle at the core of the brush border microvillus, the stoichiometry and developmental accumulation observed for espin are more compatible with a primary role for the protein in cross-linking the actin filaments together to make the parallel actin bundles of the ES junctional plaque. It is presently unclear whether other actin-bundling proteins might act in concert with espin within the ES junctional plaque. Villin appears to be absent (Robine *et al.*, 1985). And, although antibodies to fimbrin/plastin have been found to react with a protein of the expected molecular mass on Western blots of fractions enriched in ESs (Grove and Vogl, 1989), to our knowledge there have been no published reports of attempts at immunolocalization.

ACKNOWLEDGMENTS

We thank Dr. Rex Chisholm for the mouse genomic DNA library, Dr. Christine Collins and Dr. Ameet Kini for the rat testis actin-myosin, Jodi Irwin for help with DNA sequencing, Dr. Kate Spiegel for help with the analytical ultracentrifugation, and Maya Moody for help with sectioning and figure preparation. This work was supported by National Institutes of Health grant R01 HD-35280, National Institutes of Health Independent Scientist Award K02 HD-01210, and American Cancer Society grant RPG-96-094-04-CSM awarded to J.R.B.

REFERENCES

Alicea, H.A., and Mooseker, M.S. (1988). Characterization of villin from the intestinal brush border of the rat, and comparative analysis with avian villin. Cell Motil. Cytoskeleton *9*, 60–72.

Altschul, S.F., Madden, T.L., Schaffer, A.S., Zhang, J., Zhang, Z., Miller, W., and Lipman, D.J. (1997). Gapped BLAST and PSI-BLAST:

a new generation of protein database search programs. Nucleic Acids Res. *25*, 3389–3402.

Bartles, J.R., Wierda, A., and Zheng, L. (1996). Identification and characterization of espin, an actin-binding protein localized to the F-actin-rich junctional plaques of Sertoli cell ectoplasmic specializations. J. Cell Sci. *109*, 1229–1239.

Bartles, J.R., Zheng, L., Li, A., Wierda, A., and Chen, B. (1998). Small espin: a third actin-bundling protein and potential forked protein ortholog in brush border microvilli. J. Cell Biol. *143*, 107–119.

Bryan, J., and Kane, R.E. (1978). Separation and interaction of the major components of sea urchin actin gel. J. Mol. Biol. *125*, 207–224.

Beach, S.F., and Vogl, A.W. (1999). Spermatid translocation in the rat seminiferous epithelium: coupling membrane trafficking machinery to a junction plaque. Biol. Reprod. *60*, 1036–1046.

Ben Ze'ev, A., and Geiger, B. (1998). Differential molecular interactions of beta-catenin and plakoglobin in adhesion, signaling and cancer. Curr. Opin. Cell Biol. *10*, 629–639.

Burgess, D.R., Broschat, K.O., and Hayden, J.M. (1987). Tropomyosin distinguishes between the two actin-binding sites of villin and affects actin-binding properties of other brush border proteins. J. Cell Biol. *104*, 29–40.

Cesario, M.M., Ensrud, K., Hamilton, D.W., and Bartles, J.R. (1995). Biogenesis of the posterior-tail plasma membrane domain of the mammalian spermatozoon: targeting and lateral redistribution of the posterior-tail domain-specific transmembrane protein CE9 during spermiogenesis. Dev. Biol. *169*, 473–486.

Chen, H., Fre, S., Slepnev, V.I., Capua, M.R., Takei, K., Butler, M.H., Di Fiore, P.P., and De Camilli, P. (1998). Epsin is an EH-domain-binding protein implicated in clathrin-mediated endocytosis. Nature *394*, 793–797.

Cooper, J.A., and Pollard, T.D. (1982). Methods to measure actin polymerization. Methods Enzymol. *85*, 182–210.

DeRosier, D.J., and Tilney, L.G. (1981). How actin filaments pack into bundles. Cold Spring Harbor Symp. Quant. Biol. *81*, 525–540.

Edwards, R.A., Herrera-Sosa, H., Otto, J., and Bryan, J. (1995). Cloning and expression of a murine fascin homolog from mouse brain. J. Biol. Chem. *270*, 10764–10770.

Ezzell, R.M., Chafel, M.M, and Matsudaira, P.T. (1989). Differential localization of villin and fimbrin during development of the mouse visceral endoderm and intestinal epithelium. Development *106*, 407–419.

Fath, K.R., and Burgess, D.R. (1995). Microvillus assembly: not actin alone. Curr. Biol. *5*, 591–593.

Friederich, E., Vancompernolle, K., Louvard, D., and Vandekerckhove, J. (1999). Villin function in the organization of the actin cytoskeleton. Correlation of in vivo effects to its biochemical activities in vitro. J. Biol. Chem. *274*, 26751–26760.

Furukawa, R., and Fechheimer, M. (1997). The structure, function, and assembly of actin filament bundles. Int. Rev. Cytol. *175*, 29–90.

Gay, N.J., and Ntwasa, M. (1993). The Drosophila ankyrin repeat protein cactus has a predominantly α-helical secondary structure. FEBS Lett. *335*, 155–160.

Glenney, J.R., Jr., Kaulfus, P., Matsudaira, P., and Weber, K. (1981). F-actin binding and bundling properties of fimbrin, a major cytoskeletal protein of microvillus core filaments. J. Biol. Chem. *256*, 9283–9288.

Grieshaber, S., and Petersen, N.S. (1999). The *Drosophila* forked protein induces the formation of actin fiber bundles in vertebrate cells. J. Cell Sci. *112*, 2203–2211.

Grove, B.D., and Vogl, A.W. (1989). Sertoli cell ectoplasmic specializations: a new type of actin-associated adhesion junction? J. Cell Sci. *93*, 309–323.

Heintzelman, M.B., and Mooseker, M.S. (1992). Assembly of the intestinal brush border cytoskeleton. Curr. Top. Dev. Biol. *26*, 93–122.

Hoover, K.K., Chien, A.J., and Corces, V.G. (1993). Effect of transposable elements on the expression of the *forked* gene of *Drosophila melanogaster*. Genetics *135*, 507–526.

Leblond, C.P., and Clermont, Y. (1952a). Definition of the stages of the cycle of the seminiferous epithelium in the rat. Ann. NY Acad. Sci. *55*, 548–573.

Leblond, C.P., and Clermont, Y. (1952b). Spermiogenesis of rat, mouse, hamster, and guinea pig as revealed by the "periodic acid-fuschsin sulfurous acid" technique. Am. J. Anat. *90*, 167–215.

Lessard, J.L. (1988). Two monoclonal antibodies to actin: one muscle selective and one generally reactive. Cell Motil. Cytoskeleton *10*, 349–362.

Lin, C.S., Shen, W., Chen, Z.P., Tu, Y.H., and Matsudaira, P. (1994). Identification of I-plastin, a human fimbrin isoform expressed in intestine and kidney. Mol. Cell. Biol. *14*, 2457–2467.

Matsudaira, P. (1991). Modular organization of actin cross-linking proteins. Trends Biochem. Sci. *16*, 87–92.

Michaely, P., and Bennett, V. (1993). The membrane-binding domain of ankyrin contains four independently folded subdomains, each comprised of six ankyrin repeats. J. Biol. Chem. *268*, 22703–22709.

Michaely, P., and Bennett, V. (1995). The ANK repeats of erythrocyte ankyrin form two distinct but cooperative binding sites for the erythrocyte anion exchanger. J. Biol. Chem. *270*, 22050–22057.

Namba, Y., Ito, M., Zu, Y., Shigesada, K., and Maruyama, K. (1992). Human T cell L-plastin bundles actin filaments in a calcium-dependent manner. J. Biochem. *112*, 503–507.

Oko, R., Hermo, L., and Hecht, N.B. (1991). Distribution of actin isoforms within cells of the seminiferous epithelium of the rat testis: evidence for a muscle form of actin in spermatids. Anat. Rec. *231*, 63–81.

Petruszak, J.A.M., Nehme, C.L., and Bartles, J.R. (1991). Endoproteolytic cleavage in the extracellular domain of the integral plasma membrane protein CE9 precedes its redistribution from the posterior to the anterior tail of the rat spermatozoon during epididymal maturation. J. Cell Biol. *114*, 917–927.

Pollard, T.D. (1993). Actin and actin-binding proteins. In: Guidebook to the Cytoskeletal and Motor Proteins, ed. T. Kreis, and R. Vale, Oxford: Oxford University Press, 3–11.

Puius, Y.A., Mahoney, N.M., and Almo, S.C. (1998). The modular structure of actin-regulatory proteins. Curr. Opin. Cell Biol. *10*, 23–34.

Renato de Franca, L., Ghosh, S., Ye, S.-J., and Russell, L.D. (1993). Surface and surface-to-volume relationships of the Sertoli cell during the cycle of the seminiferous epithelium in the rat. Biol. Reprod. *49*, 1215–1228.

Robine, S., Huet, C., Moll, R., Sahuquiollo-Merino, C., Coudrier, E., Zweibaum, A., and Louvard, D. (1985). Can villin be used to identify malignant and undifferentiated normal digestive epithelial cells? Proc. Natl. Acad. Sci. USA *82*, 84888492.

Russell, L.D., Ettlin, R.A., Hikim, A.P.S., and Clegg, E.D. (1990). Histological and Histopathological Evaluation of the Testis, Clearwater, FL: Cache River Press.

Russell, L.D., Goh, J.C., Rashed, R.M.A., and Vogl, A.W. (1988). The consequences of actin disruption at Sertoli ectoplasmic specialization sites facing spermatids after in vivo exposure of rat testis to cytochalasin D. Biol. Reprod. *39*, 105–118.

Russell, L.D., and Peterson, R.N. (1985). Sertoli cell junctions: morphological and functional correlates. Int. Rev. Cytol. *94*, 177–211.

Sawtell, N.M., and Lessard, J.L. (1989). Cellular distribution of smooth muscle actins during mammalian embryogenesis: expression of the α-vascular but not the γ-enteric isoform in differentiating striated myocytes. J. Cell Biol. *109*, 2929–2937.

Schoenwaelder, S.M., and Burridge, K. (1999). Bidirectional signaling between the cytoskeleton and integrins. Curr. Opin. Cell Biol. *11*, 274–286.

Stokes, D.L., and DeRosier, D.J. (1991). Growth conditions control the size and order of actin bundles in vitro. Biophys. J. *59*, 456–465.

Vancompernolle, K., Vandekerchove, J., Bubb, M.R., and Korn, E.D. (1991). The interfaces of actin and *Acanthamoeba* actobindin. Identification of a new actin-binding motif. J. Biol. Chem. *266*, 15427–15431.

Vogl, A.W. (1989). Distribution and function of organized concentrations of actin filaments in mammalian spermatogenic cells and Sertoli cell. Int. Rev. Cytol. *119*, 1–56.

Vogl, A.W. (1996). Spatially dynamic intercellular adhesion junction is coupled to a microtubule-based motility system: evidence from an in vitro binding assay. Cell Motil. Cytoskeleton *34*, 1–12.

Vogl, A.W., Pfeiffer, D.C., and Redenbach, D.M. (1991). Ectoplasmic ("junctional") specializations in mammalian Sertoli cells: influence on spermatogenic cells. Ann. NY Acad. Sci. *637*, 175–202.

Yamamoto, K. (1991). Identification of the site important for the actin-activated MgATPase activity of myosin subfragment-1. J. Mol. Biol. *217*, 229–233.

Yonezawa, N., Nishida, E., Ohba, M., Seki, M., Kumagai, H., and Sakai, H. (1989). An actin-interacting heptapeptide in the cofilin sequence. Eur. J. Biochem. *183*, 235–238.

Zigmond, S.H., Furukawa, R., and Fechheimer, M. (1992). Inhibition of actin filament depolymerization by the *Dictyostelium* 30,000 dalton actin bundling protein. J. Cell Biol. *119*, 559–567.